Forecasting Evolution of Sulfide Mineral Oxidation Rates Over Decadal Time Scales

John B. Swenson[1,2], Tamara R. Diedrich[1]

[1]*MineraLogic LLC, 306 W Superior St, Duluth, MN, 55802, USA, jswenson@mnlogic.com, tdiedrich@mnlogic.com*

[2]*Department of Earth and Environmental Sciences, University of Minnesota Duluth, 1114 Kirby Dr, Duluth, MN, 55812, USA, jswenso2@d.umn.edu, ORCID 0000-0002-4238-8395*

Abstract

Leachate from 26 decadal-duration laboratory tests on tailings isolated the time-dependence of sulfide mineral oxidation from field scale sources of variability. Time series from *all* tests show a three-phase evolution, with an **order-of-magnitude decrease in sulfate release rate** during the second phase. The first phase is relatively short (0.7-yr avg.), with large, quasi-steady release rates. In the second phase – of two- to six-years duration – release rates show a power-law dependence on time. Third-phase release rates are near detection limits and quasi-steady or slowly decaying. We attribute the second evolutionary phase to an accumulation of weathering products that hinders sulfide oxidation.

Keywords: Sulfide Minerals, Pyrrhotite, Oxidation Rates, Forecasting

Introduction

Characterizations of long-term (decadal scale or longer) oxidation rates of sulfide minerals in mine waste is directly significant to forecasting contact-water chemistry over the life of mine and post-closure. Incorporating potential time dependence into the oxidation rate characterization—and, therefore, water chemistry forecasts—presents an opportunity to refine the basis for more effectively designed mine waste management systems and closure planning.

Theoretical models of time-dependent sulfide-mineral apparent reactivity have been established for mining and other applications, e.g. Wunderly *et al.* (1996). These models have been successfully applied to describe water chemistry observations across a range of mine sites. However, logistical constraints and complexities inherent of full-scale field systems, such as site-specific seasonality and stochastic fluctuations in temperature and hydrology, limit the ability to isolate the effect of time-dependent oxidation rates from other factors. Laboratory-scale experiments, while introducing uncertainty associated with upscaling results in space and time, would have the potential to eliminate much of the variability in environmental forcing. However, there have been exceedingly few opportunities to test directly these model predictions against observations from well-controlled laboratory experiments conducted over relevant (decadal) timescales.

Here we present data from a unique, industry-supported, laboratory-scale experiment of tailings oxidation. We analyzed leachate from 26 humidity-cell tests (HCTs) of exceptionally long duration (more than a decade). The time series from all HCTs show an order-of-magnitude decrease in sulfate release rates over timescales of less than a decade.

Experimental Methods

Mine waste materials analyzed here are tailings derived from a pilot-plant test program that processed 1.1 Ga, mafic (troctolitic), magmatic Cu-Ni sulfide ore from a mining project in development at the time. The dominant sulfide mineral is pyrrhotite; the tailings are characterized by relatively low overall sulfur content (< 0.15 weight percent S, as sulfide). Based on grain size (d), tailings collected at various stations in the ore-processing flow were subdivided into four classes—fine (d < 75 μm), medium (75 μm < d < 150 μm), coarse (d > 150 μm), and whole

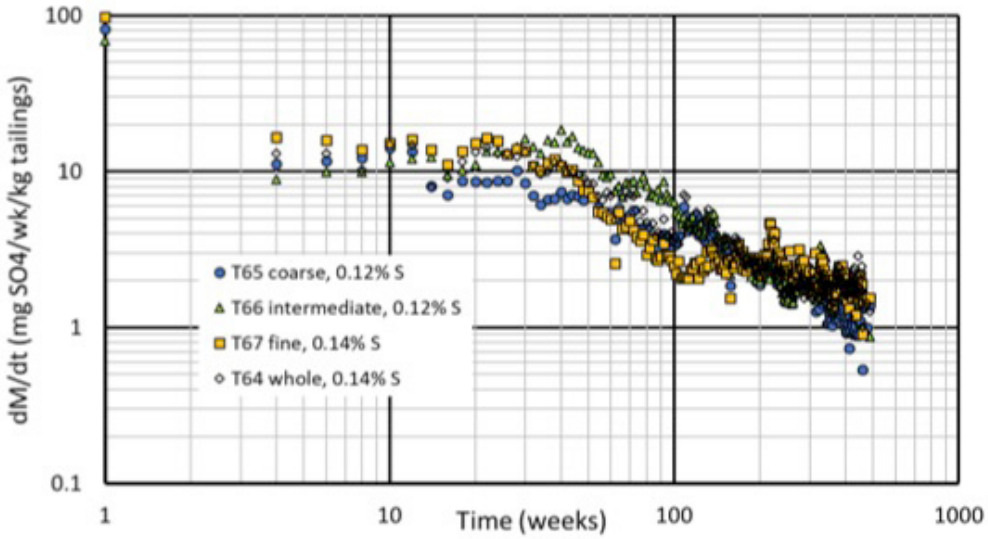

Figure 1 Times series of sulfate-release rates for HCTs T64 – T67; behavior shown here is representative of that observed in all 26 samples.

(unsorted). The 26 samples were given unique identifiers T8 – T13 and T52 – T71 (Table 1), placed in standard humidity cells, and allowed to weather under steady, controlled-climate laboratory conditions. Following ASTM (2013) standards, sample size was 1 kg of tailings, which was rinsed weekly with 500 ml of water. Collected leachate was analyzed for a suite of constituents. The duration of the weathering experiments exceeded ten years, thus providing exceptionally long time series of sulfate release rates under uniform environmental conditions, thereby eliminating the complexity of climate and seasonality that typically plagues field-based studies. Individual samples (HCTs) varied in grain size, sulfur content, but had consistent gangue mineral composition.

Experimental Results and Empirical Model

Each of the 26 sulfate-release time series, when plotted in log-log space, displays a clear break in scaling near a time t_{brk}, where t_{brk} is typically a few tens of weeks. Prior to t_{brk}, i.e. at 'early' times, the SO_4 release rate is relatively steady and large. Importantly, for $t > t_{brk}$, the release rate decays quasi-linearly in log-log space, characteristic of a power-law dependence on time. Figure 1 shows the time series of sulfate release for HCTs T64 – T67, which vary in grain size and sulfur content. The behavior shown in these four release-rate time series is representative of that in *all* 26 HCTs.

Figure 1 isolates and annotates the time series of sulfate release for HCT T67 (fine-grained, 0.14% S). Note the break in scaling at approximately 30 weeks of exposure. Based on observations common to all HCT time series, we established an empirical model of sulfate release through time:

$$\dot{M} = \begin{cases} \dot{M}_o & , \quad t_{min} < t < t_{brk} \\ C_1 t^{-\alpha} & , \quad t_{brk} < t \\ \dot{M}_\infty & , \quad C_1 t^{-\alpha} < \dot{M}_\infty \end{cases} \qquad (1)$$

where $\dot{M}$ is the time-dependent sulfate release rate (mg $SO_4 \cdot kg^{-1} \cdot wk^{-1}$); $\dot{M}_o$, C_1, and α are parameters determined from graphical analysis of each time series; and t_{min} and t_{brk} are, respectively, the time of the first observed release rate to be used in the empirical model (five weeks, per regulatory guidelines) and the end of the first model phase, which is characterized by a nearly steady release rate ($\dot{M}_o$). Parameters α and C_1 represent, respectively, the scaling exponent in a power-law relationship and the *one-week* sulfate release rate.

At very large times, e.g. $t > 200$ weeks, sulfate-release rates again break scaling, departing from the power-law relationship in Eq. 1. In general, the release rates decrease to

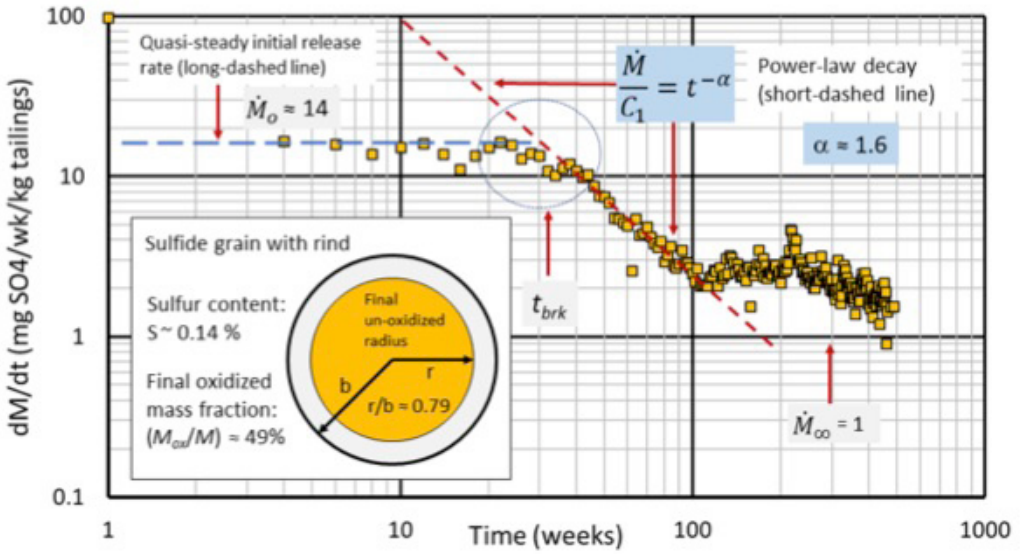

Figure 2 Annotated time series of sulfate release rate for HCT T67; inset cartoon depicts development of weathering rind.

values near 1 – 2 mg $SO_4 \cdot kg^{-1} \cdot wk^{-1}$—hovering slightly above detection limits—and show no consistent trend across the full set of time series. Pending further analysis of these large-time data, we adopt a conservative empirical modeling approach, in which the release rate is set to a constant 'floor' value ($\dot{M}_\infty$) of 1 mg $SO_4 \cdot kg^{-1} \cdot wk^{-1}$ (Eq. 1). Note that this floor applies only to the sulfate release rate model and does not imply that sulfate release continues indefinitely, as ultimately the sulfur source will be exhausted.

Table 1 provides a summary of the observed empirical model parameters, i.e. $\dot{M}_o$, C_1, and α. Tracking sulfur release through time allows straightforward computation of the mass fraction of sulfur oxidized during the experiments, M_{ox}/M, where M is the original mass of sulfur as sulfide. On average, the duration of the HCTs was sufficient to allow oxidization of approximately 50% of the original sulfur (as sulfide) mass. Assuming spherical sulfide grains, the average un-oxidized radius fraction, *r/b*, at experiment completion was 0.79 (Table 1), suggesting the development of a weathering rind in the outer 20% of the original sulfide-grain radius (Fig. 2).

The most important observational aspect of the HCT time series is the **order-of-magnitude decay** in SO_4 release rate in the two- to six-year timeframe of *all* 26 HCTs. In the following section, we present a plausible explanation for this observed decay.

Two-Phase Mathematical Model of Sulfide Oxidation

In many natural systems, a break in scaling—such as that shown in Figs. 1 and 2—commonly reflects a 'handoff' between two competing physical, chemical, or biological processes. A putative explanation of the handoff in sulfate-release rate near t_{brk} is the accumulation of oxidation products—the development of a weathering rind, in effect, composed of iron hydroxides or oxyhydroxides—on the sulfide grain of sufficient thickness to affect the rate of sulfide oxidation (Fig. 3c). Diffusion of dissolved oxygen (inbound) and SO_4 anions (outbound) across this rind is relatively inefficient and thus slows the SO_4 release rate. Continued thickening of the rind with time results in a monotonic decay in sulfate release rates, *sensu* the well-established 'shrinking core' model (Davis and Ritchie 1986). Prior to the accumulation of an appreciable thickness of oxidation byproducts, the SO_4 release rate per unit of reactive area is approximately constant, and any decay in overall sulfate release rate is driven by physical shrinking of the grain, i.e. the so-called 'shrinking

Table 1 HCT sample characteristics and best-fit model parameters.

ID	d (µm)	S %	$\dot{M}_o$	C_1	α	M_{ox}/M	r/b	t_{brk}	j_o	D
T8	>150	0.11	6	2000	1.3	0.48	0.78	90	$5.0{\cdot}10^{-10}$	$2.0{\cdot}10^{-17}$
T9	75 – 150	0.10	8	10000	1.6	0.53	0.81	70	$7.0{\cdot}10^{-10}$	$3.6{\cdot}10^{-17}$
T10	< 75	0.09	18	150	0.9	0.51	0.80	20	$1.5{\cdot}10^{-9}$	$3.1{\cdot}10^{-17}$
T11	> 150	0.11	7	2500	1.3	0.45	0.76	80	$6.0{\cdot}10^{-10}$	$1.8{\cdot}10^{-17}$
T12	75 – 150	0.14	12	7100	1.5	0.51	0.80	81	$7.0{\cdot}10^{-10}$	$1.0{\cdot}10^{-17}$
T13	< 75	0.14	20	300	0.9	0.49	0.79	20	$1.7{\cdot}10^{-9}$	$2.4{\cdot}10^{-17}$
T52	whole	0.09	9	11000	1.5	0.54	0.81	70	$8.0{\cdot}10^{-10}$	$1.3{\cdot}10^{-17}$
T53	> 150	0.10	15	200	1.1	0.48	0.78	20	$8.0{\cdot}10^{-10}$	$3.2{\cdot}10^{-17}$
T54	75 – 150	0.08	10	300	1.0	0.57	0.83	25	$1.0{\cdot}10^{-9}$	$4.0{\cdot}10^{-17}$
T55	< 75	0.10	18	400	1.1	0.55	0.82	30	$1.2{\cdot}10^{-9}$	$2.5{\cdot}10^{-17}$
T56	whole	0.10	9	300	1.0	0.47	0.78	30	$1.0{\cdot}10^{-9}$	$1.8{\cdot}10^{-17}$
T57	> 150	0.11	8	250	1.0	0.42	0.75	30	$8.0{\cdot}10^{-10}$	$1.5{\cdot}10^{-17}$
T58	75 – 150	0.08	8	300	1.0	0.53	0.81	40	$1.0{\cdot}10^{-9}$	$3.1{\cdot}10^{-17}$
T59	< 75	0.11	11	300	1.0	0.46	0.77	20	$1.3{\cdot}10^{-9}$	$2.7{\cdot}10^{-17}$
T60	whole	0.11	10	700	1.2	0.46	0.77	25	$1.0{\cdot}10^{-9}$	$2.7{\cdot}10^{-17}$
T61	> 150	0.11	8	240	1.0	0.42	0.75	20	$1.0{\cdot}10^{-9}$	$2.7{\cdot}10^{-17}$
T62	75 – 150	0.10	9	300	1.0	0.49	0.79	30	$9.0{\cdot}10^{-10}$	$2.4{\cdot}10^{-17}$
T63	< 75	0.12	14	230	1.1	0.40	0.74	20	$1.2{\cdot}10^{-9}$	$1.5{\cdot}10^{-17}$
T64	whole	0.14	13	920	1.2	0.51	0.80	30	$8.0{\cdot}10^{-10}$	$2.5{\cdot}10^{-17}$
T65	> 150	0.12	10	300	1.0	0.49	0.79	20	$8.0{\cdot}10^{-10}$	$2.5{\cdot}10^{-17}$
T66	75 – 150	0.12	13	1400	1.2	0.62	0.85	40	$1.2{\cdot}10^{-9}$	$3.7{\cdot}10^{-17}$
T67	< 75	0.14	14	1600	1.4	0.49	0.79	30	$8.5{\cdot}10^{-10}$	$1.7{\cdot}10^{-17}$
T68	whole	0.12	13	600	1.2	0.46	0.77	30	$9.0{\cdot}10^{-10}$	$1.8{\cdot}10^{-17}$
T69	> 150	0.11	8	240	1.0	0.46	0.77	20	$9.0{\cdot}10^{-10}$	$2.8{\cdot}10^{-17}$
T70	75 – 150	0.11	10	800	1.1	0.51	0.80	35	$1.0{\cdot}10^{-9}$	$3.1{\cdot}10^{-17}$
T71	< 75	0.14	12	520	1.1	0.41	0.74	20	$1.0{\cdot}10^{-9}$	$2.0{\cdot}10^{-17}$
arithmetic mean		0.11	11		1.1	0.49	0.79	36	$9.7{\cdot}10^{-10}$	$2.4{\cdot}10^{-17}$

Note on units: $\dot{M}_o$ and C1 in mg $SO_4{\cdot}kg^{-1}{\cdot}wk^{-1}$; t_{brk} in weeks; j_o in $mols{\cdot}m^{-2}{\cdot}s^{-1}$; and D in $m^2{\cdot}s^{-1}$.

particle' model (e.g., Bilenker *et al.* 2016). We developed a *hybrid* model—summarized below—for sulfate release from an idealized abstraction of an HCT that combines the shrinking-particle and shrinking-core theoretical frameworks.

In our hybrid model, the shrinking-particle framework applies early in the oxidation process, during what we term a 'tarnishing' phase (Fig. 3c). The basic assumptions underpinning the tarnishing model are 1) a constant oxidation rate per unit area of reactive surface on the sulfide grain and 2) insufficient accumulation of oxidation products, e.g. FeO(OH) minerals, to affect the oxidation rate. The constant oxidation rate is embodied in a dissolution flux (j_o; $mols{\cdot}m^{-2}{\cdot}s^{-1}$) of sulfate anions leaving the reactive surface of the sulfide grain. With no accumulation of oxidation products, the diameter of the reactive surface and, by extension, the grain itself must decrease with time, hence the 'shrinking particle' nomenclature (Fig. 3c). HCT data suggest that the size of the sulfide grain at the end of the tarnishing phase (b) has decreased only slightly from its initial size (b_o), i.e. $b_o \approx b$ (Fig. 3c).

The dissolution flux (j_o) depends on the detailed geochemistry of the pore fluid coating the sulfide grain and thus varies with the mineralogy of the parent rock (dominantly troctolite, in this case). While the literature provides broad and useful constraints on jo for pyrrhotite, e.g. Rimstidt (2014) and Bilenker *et al.* (2016), no independent study has constrained the kinetics underpinning j_o for the proprietary tailings we analyzed here. Given this knowledge gap, j_o is treated as a tuned parameter.

The dissolution flux (j_o) depends on the detailed geochemistry of the pore fluid coating the sulfide grain and thus varies with the mineralogy of the parent rock (dominantly troctolite, in this case). While the literature provides broad and useful constraints on

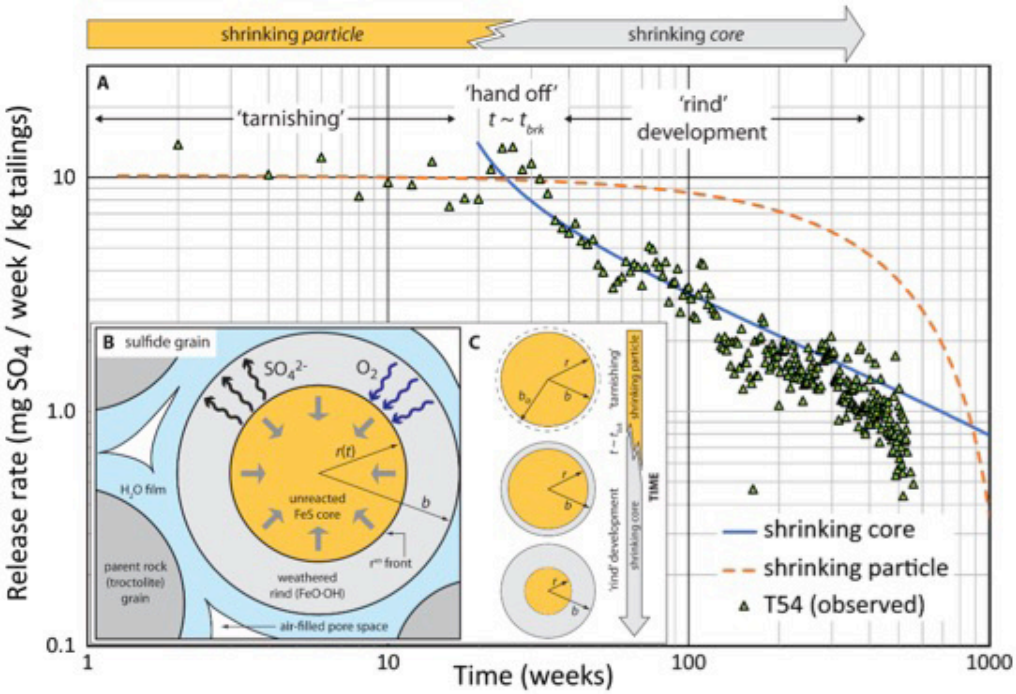

Figure 3 *(a) Observed time series of SO4 release rate for HCT T54, with best-fit shrinking-particle (orange) and shrinking-core (blue) predictions overlaid; (b) conceptual sketch of sulfide-grain weathering; and (c) cartoon illustrating transition from tarnishing phase to rind-development phase in hybrid model.*

j_o for pyrrhotite, e.g. Rimstidt (2014) and Bilenker *et al*. (2016), no independent study has constrained the kinetics underpinning j_o for the proprietary tailings we analyzed here. Given this knowledge gap, j_o is treated as a tuned parameter.

In our model, as the exposure time nears t_{brk}, the 'tarnishing' phase transitions to the 'rind development' phase, thus signifying the handoff from shrinking-particle to shrinking-core framework (Fig. 3). The primary differentiating feature of the latter is its treatment of the Fe-bearing oxidation byproducts, which are assumed to *remain attached* to the grain in the form of an FeO(OH) mineral rind, through which oxygen must diffuse to reach the reactive surface of the shrinking 'core' of unreacted FeS, *sensu* Davis and Ritchie (1986) and Wunderly *et al*. (1996). Likewise, sulfate must diffuse outward through the rind to reach the water film coating the sulfide grain. Throughout this model phase, the overall radius (b) of the affected grain remains steady, but the radius of the unreacted FeS core, r(t), decays with time, while, by extension, the thickness of the rind, b-r, increases with time. Diffusion of oxygen through the rind is slow relative to oxidation of pyrrhotite at the reactive outer surface of the core, which is treated as a 'sharp' front; there is no O_2 consumption in the FeO(OH) rind, i.e. oxidation is complete, and diffusion proceeds in a quasi-steady manner, characterized by a constant and uniform diffusivity D ($m^2 \cdot s^{-1}$). The shrinking-core model, as developed here, contains a pair of tuned parameters: The onset of diffusion-controlled oxidation (t_{brk}) and the diffusivity D of the weathering rind. Both parameters are determined by subjective 'best fits' to the observed SO_4 release-rate time series from HCTs.

Our hybrid model does not address the observed second break in scaling at very large times, as this behavior is beyond project scope. Multiple plausible explanations exist for this apparent handoff to a third set of processes: A likely candidate is pore-scale 'poisoning' of the system via incomplete removal of weathering byproducts and/or precipitation of secondary minerals.

Model Results and Interpretation

Application of our hybrid model to the observed HCT time series is relatively straightforward. The model framework described above applies to an individual sulfide grain. Upscaling to the overall sulfate release rate from an HCT—and its ensemble of sulfide grains—involves determination of the number of sulfide grains based on bulk sulfur content and sulfide grain size. Consider the observed sulfate-release rates from HCT T54 shown in Figure 3a. By inspection, the break in scaling occurs approximately 20 – 30 weeks into the experiment. With 0.08% S and an assumed sulfide particle size of 20 μm, a dissolution flux (j_o) of $1 \cdot 10^{-9}$ mol·m^{-2}·s^{-1} yields a reasonable fit (dashed curve in Fig. 3a) to the observed data from the 'tarnishing' phase of the experiment. This estimate of j_o is similar to that reported by Bilenker *et al.* (2016) for pyrrhotite in slightly acidic waters (jo = $1.5 \cdot 10^{-9}$ mol·m^{-2}·s^{-1}; pH = 6). With jo constrained from the tarnishing-phase data, simultaneous adjustment of t_{brk} (i.e., 'fine tuning' relative to the initial visual estimate of 20 – 30 weeks) and diffusivity, D, gives a subjective best fit (solid curve in Fig. 3a) to the HCT data for parameter values t_{brk} = 25 weeks and D = $2 \cdot 10^{-17}$ m^2·s^{-1}. This diffusivity is consistent with values reported in the literature (e.g. Wunderly *et al.* 1996). Table 1 contains the values of j_o, D, and t_{brk} obtained by repeating this fitting exercise for the remaining 25 HCT time series.

Discussion and Conclusions

By minimizing environmental variability, the long-duration HCT data we present here provide important insight about the time dependence of *grain-scale* oxidation processes. All sulfate-release-rate time series we analyzed share a common and critically important attribute—an order-of-magnitude decrease in SO_4 release rate on decadal timescales, preceded by a relatively short interval of nearly steady release. The ubiquity of this two-phase behavior motivated our development of a *grain-scale* hybrid model that provides a putative explanation for the onset of decay in release rate.

When nested within a site-specific, vadose-zone hydrologic model, our hybrid oxidation model may improve ability to forecast mine water quality over multi-decadal time scales, with attendant implications for mine permitting. While upscaling experimental insight to the mine scale poses well-recognized challenges, utilization of a simple intermittency factor—to reflect seasonality in cool, temperate climates—suggests that the order-of-magnitude decrease in sulfate release rate would be realized within a few decades of mine closure; warmer climates with less seasonality may realize this decrease earlier.

Acknowledgements

We gratefully acknowledge Stephen Day and others at SRK for their contributions to design and oversight of the kinetic test program utilized here.

References

ASTM (2013) Standard Test Method for Laboratory Weathering of Solid Materials Using a Humidity Cell. D5744-13

Bilenker LD, Romano GY, McKibben MA (2016) Kinetics of sulfide mineral oxidation in seawater: Implications for acid generation during in situ mining of seafloor hydrothermal vent deposits. Applied Geochemistry, 75, doi: 10.1016/j.apgeochem.2016.10.010

Davis G, Ritchie A (1986) A model of oxidation in pyritic mine wastes: part 1, equations and approximate solution. Applied Mathematical Modelling, 10(5): 314 – 322

Rimstidt JD (2014) Geochemical Rate Models: An Introduction to Geochemical Kinetics. Cambridge University Press. DOI:https://doi.org/10.1017/CBO9781139342773

Wunderly M, Blowes DW, Frind EO, Ptacek CJ (1996) Sulfide mineral oxidation and subsequent reactive transport of oxidation products in mine tailings impoundments: A numerical model. Water Resources Research, 32(10)